Paper:

Dynamical Model of Walking Transition Considering Nonlinear Friction with Floor

Xiang Li, Hiroki Imanishi, Mamoru Minami, Takayuki Matsuno, and Akira Yanou

Graduate School of Nature Science and Technology, Okayama University
3-1-1 Tsushima-naka, Kita-ku, Okayama, Okayama 700-8530, Japan
E-mail: pzkm87r2@s.okayama-u.ac.jp
[Received February 29, 2016; accepted August 17, 2016]

Biped locomotion created by a controller based on Zero-Moment Point (ZMP) known as reliable control method looks different from human's walking on the view point that ZMP-based walking does not include falling state, and it's like monkey walking because of knee-bended walking profiles. However, the walking control that does not depend on ZMP is vulnerable to turnover. Therefore, keeping the event-driven walking of dynamical motion stable is important issue for realization of human-like natural walking. In this research, a walking model of humanoid robot including slipping, bumping, surface-contacting and line-contacting of foot is discussed, and its dynamical equation is derived by the Extended NE method. In this paper we introduce the humanoid model which including the slipping foot and verify the model.

Keywords: humanoid, slipping, friction, bipedal, dynamical

1. Introduction

Human beings have acquired an ability of stable bipedal walking in evolving repetitions so far. From a view point of making a stable controller for the bipedal walking based on knowledge of control theory is not easy, because of the dynamics with high nonlinearity and coupled interactions between state variables with high dimensions. Therefore how to simplify the complicated walking dynamics to help construct stable walking controller has been studied intensively.

To avoiding complications in dealing directly with true dynamics (without approximation), inverted pendulum has been used frequently for making a stable controller [1–3], simplifying the calculations to determine input torque. Further, linear approximation having the humanoid being represented by simple inverted pendulum enables researchers to realize stable gait through well-known control strategy [4–6].

Our research has begun from a view point of [7, 8] as aiming to describing gait's dynamics as correctly as possible, including point-contacting state of foot and toe, slipping of the foot and bumping. We discuss the dynamics of whole-body humanoid that contains head, waist and arms. And that what we think more important is that the dimension of dynamical equation will change depending on the walking gait's varieties, which has been discussed by [9] about concerning one legged hopping robot. In fact, this kind of dynamics with the dimension number of state variables varying by the result of its dynamical time transitions that are out of the arena of control theory that discusses how to control a system with fixed states' number. Further the tipping over motion has been called as non-holonomic dynamics that includes a joint without inputting torque, i.e., free joint.

Meanwhile, landing of the heel or the toe of lifting leg in the air to the ground makes a geometrical contact. Based on [10]. We derive the dynamics of humanoid which is simulated as a serial-link manipulator including constraint motion and slipping motion by using the Extended Newton-Euler Method [11].

The conventional method of the NE could be applied to a robot having an open loop serial linkage structure, but the motion of hand was limited to motions without contacting external world. The NE method has not been formulated although it was very important for a robot that works under a premise it must be contacted with the environment when the robot was doing some grinding work or assembling work. For this point, the extended NE method was proposed in [11] that is as same as the research of [12], in terms of that the constraints are strictly satisfied. Meanwhile, the constraint force which can be included in the iterative calculation of the NE method by calculating the constraint force by a substitution method [13].

In this research that based on [14, 15], a walking model of humanoid robot including slipping, bumping, surface-contacting and point-contacting of foot is discussed, and its dynamical equation is derived by the NE method. Especially the common consideration of the free-leg model [16–18] is without any slipping. This research is different from the conventional consideration, that the nonlinear friction which includes the static/kinetic friction will be discussed in walking model of humanoid model.

In this paper, a dynamical model of humanoid including influences of nonlinearity caused by stick-slip [19–21] motions, which are derived from the nonlinear friction between the floor and humanoid's feet, will be introduced.

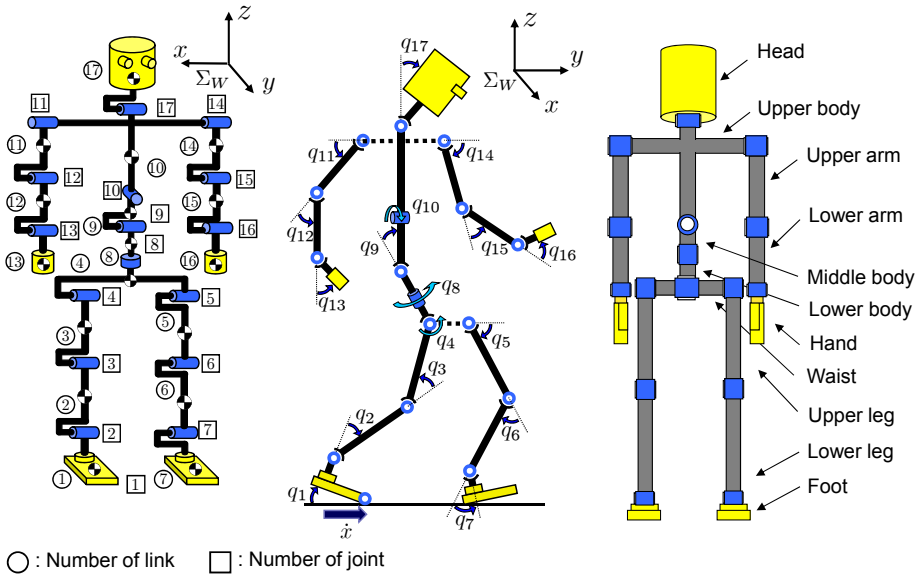

Fig. 1. Definition of humanoid's link, joint and whole body.

Table 1. Physical parameters.

Link	l_i	m_i	d_i
Head	0.24	4.5	0.5
Upper body	0.41	21.5	10.0
Middle body	0.1	2.0	10.0
Lower body	0.1	2.0	10.0
Upper arm	0.31	2.3	0.03
Lower arm	0.24	1.4	1.0
Hand	0.18	0.4	2.0
Waist	0.27	2.0	10.0
Upper leg	0.38	7.3	10.0
Lower leg	0.40	3.4	10.0
Foot	0.07	1.3	10.0
Total weight [kg]	—	64.2	—
Total hight [m]	1.7	—	—

Furthermore, as the preparation of walking simulation, some gaits models and their transition conditions will also be introduced.

2. Dynamical Walking Model by Newton-Euler Method

2.1. Forward Kinematical Calculations

We discuss a biped robot whose definition is depicted in **Fig. 1**. **Table 1** indicates length l_i [m], mass m_i [kg] of links and coefficient of joints' viscous friction d_i [N·m·s/rad], which are decided based on [22]. This model is simulated as a serial-link manipulator having ramifications and represents rigid whole body – feet including toe, torso, arms and so on – by 17 degree-of-freedom. Though motion of legs is restricted in sagittal plane, it generates varieties of walking gait sequences since the robot has flat-sole feet and kicking torque. In this paper, one foot including link-1 is defined as "supporting-leg" and another foot including link-7 is defined as "free-leg" ("contacting-leg" when the free-leg contacts with floor) according to the walking state.

In this paper, we derive the equation of motion following by NE formulation [22, 23]. So we must consider the structure of the supporting-leg with two situations. When the supporting-leg is constituted by rotating joint: We first have to calculate relations of positions, velocities and accelerations between links as forward kinetics procedures from bottom link to top link. Serial link's angular velocity ${}^i\boldsymbol{\omega}_i$, angular acceleration ${}^i\dot{\boldsymbol{\omega}}_i$, acceleration of the origin ${}^i\ddot{\boldsymbol{p}}_i$ and acceleration of the center of mass ${}^i\ddot{\boldsymbol{s}}_i$ based on Σ_i fixed at i-th link are obtained as follows.

$$ {}^i\boldsymbol{\omega}_i = {}^{i-1}\boldsymbol{R}_i^T\ {}^{i-1}\boldsymbol{\omega}_{i-1} + \boldsymbol{e}_{z_i}\dot{q}_i \quad \ldots\ldots\ldots \quad (1) $$

$$ {}^i\dot{\boldsymbol{\omega}}_i = {}^{i-1}\boldsymbol{R}_i^T\ {}^{i-1}\dot{\boldsymbol{\omega}}_{i-1} + \boldsymbol{e}_z\ddot{q}_i + {}^i\boldsymbol{\omega}_i \times (\boldsymbol{e}_{z_i}\dot{q}_i) \quad . \quad (2) $$

$$ {}^i\ddot{\boldsymbol{p}}_i = {}^{i-1}\boldsymbol{R}_i^T \left\{ {}^{i-1}\ddot{\boldsymbol{p}}_{i-1} + {}^{i-1}\dot{\boldsymbol{\omega}}_{i-1} \times {}^{i-1}\hat{\boldsymbol{p}}_i + {}^{i-1}\boldsymbol{\omega}_{i-1} \times ({}^{i-1}\boldsymbol{\omega}_{i-1} \times {}^{i-1}\hat{\boldsymbol{p}}_i) \right\} \quad \ldots\ldots \quad (3) $$

$$ {}^i\ddot{\boldsymbol{s}}_i = {}^i\ddot{\boldsymbol{p}}_i + {}^i\dot{\boldsymbol{\omega}}_i \times {}^i\hat{\boldsymbol{s}}_i + {}^i\boldsymbol{\omega}_i \times ({}^i\boldsymbol{\omega}_i \times {}^i\hat{\boldsymbol{s}}_i) \quad \ldots\ldots \quad (4) $$

Then if the supporting-leg is constituted by prismatic joint. We will switch the equations as the following.

$$ {}^i\boldsymbol{\omega}_i = {}^{i-1}\boldsymbol{R}_i^{\mathrm{T}}\ {}^{i-1}\boldsymbol{\omega}_{i-1} \quad \ldots\ldots\ldots\ldots \quad (5) $$

$$ {}^i\dot{\boldsymbol{\omega}}_i = {}^{i-1}\boldsymbol{R}_i^{\mathrm{T}}\ {}^{i-1}\dot{\boldsymbol{\omega}}_{i-1} \quad \ldots\ldots\ldots\ldots \quad (6) $$

$$ {}^i\ddot{\boldsymbol{p}}_i = {}^{i-1}\boldsymbol{R}_i^{\mathrm{T}} \left\{ {}^{i-1}\ddot{\boldsymbol{p}}_{i-1} + {}^{i-1}\dot{\boldsymbol{\omega}}_{i-1} \times {}^{i-1}\hat{\boldsymbol{p}}_i + {}^{i-1}\boldsymbol{\omega}_{i-1} \times ({}^{i-1}\boldsymbol{\omega}_{i-1} \times {}^{i-1}\hat{\boldsymbol{p}}_i) \right\} + 2({}^{i-1}\boldsymbol{R}_i^{T\,i-1}\boldsymbol{\omega}_{i-1}) \times (\boldsymbol{e}_z\dot{q}_i) + \boldsymbol{e}_z\ddot{q}_i \quad \ldots \quad (7) $$

$$ {}^i\ddot{\boldsymbol{s}}_i = {}^i\ddot{\boldsymbol{p}}_i + {}^i\dot{\boldsymbol{\omega}}_i \times {}^i\hat{\boldsymbol{s}}_i + {}^i\boldsymbol{\omega}_i \times ({}^i\boldsymbol{\omega}_i \times {}^i\hat{\boldsymbol{s}}_i) \quad \ldots\ldots \quad (8) $$

Here, ${}^{i-1}\boldsymbol{R}_i$ means orientation matrix, ${}^{i-1}\hat{\boldsymbol{p}}_i$ represents position vector from the origin of $(i-1)$-th link to the one of i-th, ${}^i\hat{\boldsymbol{s}}_i$ is defined as gravity center position of i-th link and $\boldsymbol{e}_{z_i}$ is unit vector that shows rotational axis of i-th link. However, velocity and acceleration of 4th link transmit to 8th link and ones of 10th link transmit to 11th, 14th and 17th link directly because of ramification mechanisms.

2.2. Backward Inverse Dynamical Calculations

After the above forward kinetic calculation has been done, contrarily inverse dynamical calculation from top to base link are shown as follow. Newton equation and Euler equation of i-th link are represented by Eqs. (9), (10) when ${}^i\boldsymbol{I}_i$ is defined as inertia tensor of i-th link. Here, ${}^i\boldsymbol{f}_i$ and ${}^i\boldsymbol{n}_i$ in Σ_i show the force and moment exerted on i-th link from $i+1$-th link.

$$ {}^i\boldsymbol{f}_i = {}^i\boldsymbol{R}_{i+1}\ {}^{i+1}\boldsymbol{f}_{i+1} + m_i\,{}^i\ddot{\boldsymbol{s}}_i \quad \ldots\ldots\ldots \quad (9) $$

$$
\begin{aligned}
{}^i\boldsymbol{n}_i = {}^i\boldsymbol{R}_{i+1}{}^{i+1}\boldsymbol{f}_{i+1} + {}^i\boldsymbol{I}_i{}^i\dot{\boldsymbol{\omega}}_i + {}^i\boldsymbol{\omega}_i \times ({}^i\boldsymbol{I}_i{}^i\boldsymbol{\omega}_i) \\
+ {}^i\hat{\boldsymbol{s}}_i \times (m_i{}^i\ddot{\boldsymbol{s}}_i) + {}^i\hat{\boldsymbol{p}}_{i+1} \times ({}^i\boldsymbol{R}_{i+1}{}^{i+1}\boldsymbol{f}_{i+1}) \quad (10)
\end{aligned}
$$

On the other hand, since force and torque of 5th and 8th links are exerted on 4th link, effects onto 4th link as:

$$
{}^4\boldsymbol{f}_4 = {}^4\boldsymbol{R}_5{}^5\boldsymbol{f}_5 + {}^4\boldsymbol{R}_8{}^8\boldsymbol{f}_8 + m_4{}^4\ddot{\boldsymbol{s}}_4, \quad \ldots\ldots \quad (11)
$$

$$
\begin{aligned}
{}^4\boldsymbol{n}_4 = {}^4\boldsymbol{R}_5{}^5\boldsymbol{n}_5 + {}^4\boldsymbol{R}_8{}^8\boldsymbol{n}_8 + {}^4\boldsymbol{I}_4{}^4\dot{\boldsymbol{\omega}}_4 + {}^4\boldsymbol{\omega}_4 \times ({}^4\boldsymbol{I}_4{}^4\boldsymbol{\omega}_4) \\
+ {}^4\hat{\boldsymbol{s}}_4 \times (m_4{}^4\ddot{\boldsymbol{s}}_4) + {}^4\hat{\boldsymbol{p}}_5 \times ({}^4\boldsymbol{R}_5{}^5\boldsymbol{f}_5) \\
+ {}^4\hat{\boldsymbol{p}}_8 \times ({}^4\boldsymbol{R}_8{}^8\boldsymbol{f}_8). \quad \ldots\ldots \quad (12)
\end{aligned}
$$

Similarly, force and torque of 11th, 14th and 17th links transmit to 10th link directly. Then, rotational motion equation of i-th link is obtained as Eq. (13) by making inner product of induced torque onto the i-th link's unit vector $\boldsymbol{e}_{z_i}$ around rotational axis:

$$
\tau_i = \boldsymbol{e}_{z_i}^T{}^i\boldsymbol{n}_i + d_i\dot{q}_i. \quad \ldots\ldots \quad (13)
$$

However, when the supporting-leg (1-st link) is slipping (prismatic joint), the torque onto the 1-st link can be calculated by following equation.

$$
f_1 = \boldsymbol{e}_{z_1}^T{}^1\boldsymbol{f}_1 + \mu_k\dot{y}_0. \quad \ldots\ldots \quad (14)
$$

Finally, we get motion equation with one leg standing as:

$$
\boldsymbol{M}(\boldsymbol{q})\ddot{\boldsymbol{q}} + \boldsymbol{h}(\boldsymbol{q},\dot{\boldsymbol{q}}) + \boldsymbol{g}(\boldsymbol{q}) + \boldsymbol{D}\dot{\boldsymbol{q}} = \boldsymbol{\tau}, \quad \ldots\ldots \quad (15)
$$

Here, $\boldsymbol{\tau} = [f_1, \tau_1, \tau_2, \cdots, \tau_{17}]$ is input torque, $\boldsymbol{M}(\boldsymbol{q})$ is inertia matrix, both of $\boldsymbol{h}(\boldsymbol{q},\dot{\boldsymbol{q}})$ and $\boldsymbol{g}(\boldsymbol{q})$ are vectors which indicate Coriolis force, centrifugal force and gravity. When the supporting-leg is slipping, the $\boldsymbol{D} = diag[\mu_k, d_1, d_2, \cdots, d_{17}]$ is a matrix which means coefficients of joints and between foot and ground. And $\boldsymbol{q} = [y_0, q_1, q_2, \cdots, q_{17}]^T$ means the angle of joints and the relative position between foot and ground. When the supporting-leg is slipping, the variable vector $\boldsymbol{q}$ consists of $\boldsymbol{q} = [y_0, q_1, q_2, \cdots, q_{17}]^T$. The viscous friction of y-axis (slipping axis) can be described as $\mu_k\dot{y}_0$ that is included in left-side of Eq. (15), and the nonlinear force generated by reaction force to the supporting-leg f_{t0} is made by $f_{t0} = \mu_k f_{n0}$ where f_{n0} is normal force exerting to supporting-leg caused by dynamical coupling of the humanoid body given by Eqs. (9) and (10), and μ_k is dynamical friction coefficient.

2.3. Constraint Conditions for Free-Leg Model

Making Free-leg contact with ground, free-leg appears with the position z_h or angle q_e to the ground being constrained. Also, when free-leg's velocity in traveling direction $\dot{y}_h$ is less than 0.01[m/s], the free-leg will be constrained in acceleration by the static friction. The constraints of foot's z-axis position, heel's rotation and foot's y-axis position can be defined as C_1, C_2 and C_3 respectively, these constraints can be written as follow, where $\boldsymbol{r}(\boldsymbol{q})$ means the free-leg's heel or toe position in Σ_W.

$$
\boldsymbol{C}(\boldsymbol{r}(\boldsymbol{q})) = \begin{bmatrix} C_1(\boldsymbol{r}(\boldsymbol{q})) \\ C_2(\boldsymbol{r}(\boldsymbol{q})) \\ C_3(\boldsymbol{r}(\boldsymbol{q})) \end{bmatrix} = \boldsymbol{0} \quad \ldots\ldots \quad (16)
$$

Then, robot's equation of motion with external force f_{nz}, friction force f_t, external torque τ_n and external force f_{ny} corresponding to C_1, C_2 and C_3 can be derived as:

$$
\begin{aligned}
\boldsymbol{M}(\boldsymbol{q})\ddot{\boldsymbol{q}} + \boldsymbol{h}(\boldsymbol{q},\dot{\boldsymbol{q}}) + \boldsymbol{g}(\boldsymbol{q}) + \boldsymbol{D}\dot{\boldsymbol{q}} \\
= \boldsymbol{\tau} + \boldsymbol{j}_{cz}^T f_{nz} - \boldsymbol{j}_t^T f_t + \boldsymbol{j}_r^T \tau_n + \boldsymbol{j}_{cy}^T f_{ny} \quad \ldots \quad (17)
\end{aligned}
$$

where $\boldsymbol{j}_{cz}$, $\boldsymbol{j}_t$, $\boldsymbol{j}_r$ and $\boldsymbol{j}_{cy}$ are defined as:

$$
\begin{aligned}
\boldsymbol{j}_{cz}^T = \left(\frac{\partial C_1}{\partial \boldsymbol{q}^T}\right)^T \left(\frac{1}{\left\|\frac{\partial C_1}{\partial \boldsymbol{r}^T}\right\|}\right), \quad \boldsymbol{j}_t^T = \left(\frac{\partial \boldsymbol{r}}{\partial \boldsymbol{q}^T}\right)^T \frac{\dot{\boldsymbol{r}}}{\|\dot{\boldsymbol{r}}\|}, \\
\boldsymbol{j}_r^T = \left(\frac{\partial C_2}{\partial \boldsymbol{q}^T}\right)^T \left(\frac{1}{\left\|\frac{\partial C_2}{\partial \boldsymbol{q}^T}\right\|}\right), \quad \boldsymbol{j}_{cy}^T = \left(\frac{\partial C_3}{\partial \boldsymbol{q}^T}\right)^T \left(\frac{1}{\left\|\frac{\partial C_3}{\partial \boldsymbol{q}^T}\right\|}\right). \quad (18)
\end{aligned}
$$

It is common sense that (i) f_{nz} and f_t are orthogonal, and (ii) value of f_t is decided by $f_t = K f_{nz}$ $(0 < K \leq 1)$. The differentiating Eq. (16) by time for two times, we can derive the constraint condition of $\ddot{\boldsymbol{q}}$.

$$
\left(\frac{\partial C_i}{\partial \boldsymbol{q}^T}\right)\ddot{\boldsymbol{q}} + \dot{\boldsymbol{q}}^T \left\{\frac{\partial}{\partial \boldsymbol{q}}\left(\frac{\partial C_i}{\partial \boldsymbol{q}^T}\right)\dot{\boldsymbol{q}}\right\} = 0 \quad \ldots \quad (19)
$$
$$
(i = 1,\ 2)
$$

Making the $\ddot{\boldsymbol{q}}$ in Eqs. (17) and (20) be identical, we can obtain the equation of contacting motion as follow.

$$
\begin{aligned}
&\begin{bmatrix} \boldsymbol{M}(\boldsymbol{q}) & -(\boldsymbol{j}_{cz}^T - \boldsymbol{j}_t^T K) & -\boldsymbol{j}_r^T & -\boldsymbol{j}_{cy}^T \\ \frac{\partial C_1}{\partial \boldsymbol{q}^T} & 0 & 0 & 0 \\ \frac{\partial C_2}{\partial \boldsymbol{q}^T} & 0 & 0 & 0 \\ \frac{\partial C_3}{\partial \boldsymbol{q}^T} & 0 & 0 & 0 \end{bmatrix} \begin{bmatrix} \ddot{\boldsymbol{q}} \\ f_{nz} \\ \tau_n \\ f_{ny} \end{bmatrix} \\
&= \begin{bmatrix} \boldsymbol{\tau} - \boldsymbol{h}(\boldsymbol{q},\dot{\boldsymbol{q}}) - \boldsymbol{g}(\boldsymbol{q}) - \boldsymbol{D}\dot{\boldsymbol{q}} \\ -\dot{\boldsymbol{q}}^T\left\{\frac{\partial}{\partial \boldsymbol{q}}\left(\frac{\partial C_1}{\partial \boldsymbol{q}^T}\right)\right\}\dot{\boldsymbol{q}} \\ -\dot{\boldsymbol{q}}^T\left\{\frac{\partial}{\partial \boldsymbol{q}}\left(\frac{\partial C_2}{\partial \boldsymbol{q}^T}\right)\right\}\dot{\boldsymbol{q}} \\ -\dot{\boldsymbol{q}}^T\left\{\frac{\partial}{\partial \boldsymbol{q}}\left(\frac{\partial C_3}{\partial \boldsymbol{q}^T}\right)\right\}\dot{\boldsymbol{q}} \end{bmatrix} \quad (20)
\end{aligned}
$$

2.4. Calculation of Bumping

When swing-leg attaches to ground, we need to consider bumping motion. There are two kinds of bumping concerning heel and toe. We denote dynamics of bumping between the heel and the ground below. By integrating Eq. (17) under $\tau_n = 0$ in time, equation of striking moment can be obtained as follows.

$$
\boldsymbol{M}(\boldsymbol{q})\dot{\boldsymbol{q}}(t_1^+) = \boldsymbol{M}(\boldsymbol{q})\dot{\boldsymbol{q}}(t_1^-) + (\boldsymbol{j}_c^T - \boldsymbol{j}_t^T K)F_{im}. \quad (21)
$$

Eq. (21) describes the bumping in z-axis of Σ_W between the heel and the ground. $\dot{\boldsymbol{q}}(t_1^+)$ and $\dot{\boldsymbol{q}}(t_1^-)$ are angular velocity after and before the strike respectively.

$$
F_{im} = \lim_{t_1^- \to t_1^+} \int_{t_1^-}^{t_1^+} f_n dt \quad \ldots\ldots \quad (22)
$$

F_{im} in Eq. (22) means impulse of bumping. Motion of the robot is constrained by the followed equation that is given by differentiating C_1 by time after the strike.

$$\frac{\partial C_1}{\partial \boldsymbol{q}}\dot{\boldsymbol{q}}(t_1^+) = 0 \quad \ldots\ldots\ldots\ldots\ldots\ldots \quad (23)$$

Then, the equation of matrix formation in the case of heel's bumping can be obtained as follows.

$$\begin{bmatrix} \boldsymbol{M}(\boldsymbol{q}) & -(\boldsymbol{j}_c^T - \boldsymbol{j}_t^T K) \\ \dfrac{\partial C_1}{\partial \boldsymbol{q}^T} & 0 \end{bmatrix} \begin{bmatrix} \dot{\boldsymbol{q}}(t_1^+) \\ F_{im} \end{bmatrix} = \begin{bmatrix} \boldsymbol{M}(\boldsymbol{q})\dot{\boldsymbol{q}}(t_1^-) \\ 0 \end{bmatrix} \quad \ldots \quad (24)$$

We can derive the dynamics regarding the toe's bumping based on the similar above process.

3. Validation of Model

3.1. Verification by Mechanical Energy

To verify this complex model, we use the mechanical energy conservation law. Because to verify the conservation of mechanical energy, the equation of motion must be correct. We make the model to do a free fall with the input torque $\boldsymbol{\tau}_i = 0$ and the viscous friction $\boldsymbol{D}_i = 0$. In this case, there is no friction. So, it will has no discharge of energy during free fall. During the motion the mechanical energy will be saved at the initial potential energy. To derive the mechanical energy, it is necessary to calculate all of the potential energy, rotational energy and translational energy.

3.2. Calculation of Mechanical Energy

It is necessary to calculate the height of the center of gravity of each link before the calculation of the potential energy. We use the homogeneous transformation matrix to calculate it as following equation.

$${}^W z_{Gi} = {}^W z_i + \frac{{}^W z_{i+1} - {}^W z_i}{2} \quad \ldots\ldots\ldots \quad (25)$$

Here, ${}^W z_{Gi}$ means the height of C.o.G of i-th link in world coordinate system ${}^W z_i$ is the height of the joint which seen from the world coordinate. So, we can calculate the potential energy as following equation.

$$E_p = \sum_{i=1}^{17} m_i {}^W z_i g \quad \ldots\ldots\ldots\ldots\ldots \quad (26)$$

Here, E_p is the potential energy of the model. m_i is the mass of each link. g is the gravitational acceleration. Then, we can calculate the rotational energy as following equation.

$$E_k = \sum_{i=1}^{17} \frac{1}{2} {}^W \boldsymbol{\omega}_i^T {}^W \boldsymbol{I}_i {}^W \boldsymbol{\omega}_i \quad \ldots\ldots\ldots \quad (27)$$

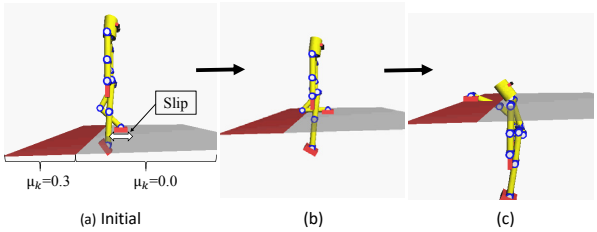

Fig. 2. Simulation environment and configuration in (a) was detected at the time designated by Ⓐ in **Fig. 3**, and also (b) and (c) are the shapes at Ⓑ and Ⓒ.

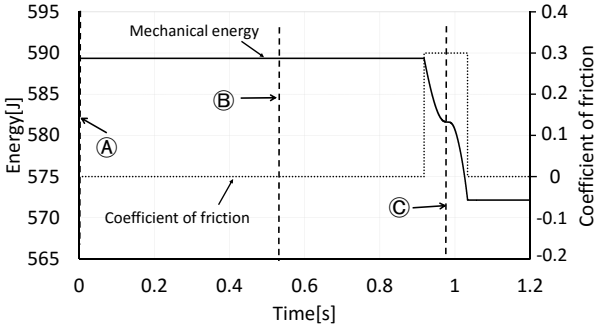

Fig. 3. Discharge of mechanical energy by friction.

Here, E_k is the rotational energy of the model. $\boldsymbol{I}_i$ is the moment of inertia of each link. Then, we can also calculate the translational energy as following equation.

$$E_v = \sum_{i=1}^{17} \frac{1}{2} m_i {}^W \dot{\boldsymbol{r}}_{gi}^T {}^W \dot{\boldsymbol{r}}_{gi} \quad \ldots\ldots\ldots \quad (28)$$

Here, E_v is the translational energy of the model, $\dot{\boldsymbol{r}}_{gi}$ is the translational velocity of C.o.G of i-th link. Finally, the mechanical energy can be derived as following equation.

$$E_Q = E_p + E_k + E_v \quad \ldots\ldots\ldots\ldots \quad (29)$$

3.3. Verification Simulation Experiment

3.3.1. Simulation Including Free-Fall

To verify this model and check the effect of the friction on the slip motion. The simulation environment is set as shown in **Fig. 2**.

The initial conditions of experiment are shown as follow. The joint angle of the whole body are set to $\boldsymbol{q} = \boldsymbol{0}$, and there are no viscous friction ($\boldsymbol{D} = \boldsymbol{0}$) and input torque ($\boldsymbol{\tau} = \boldsymbol{0}$). And the supporting-leg is constrained to ground with a surface-contact. So, the body of humanoid robot will fall freely, and the supporting-leg of Humanoid robot will have a slip motion on the ground. Because the coefficient of friction of the left side of the ground (darker part in **Fig. 2**) is set to $\mu_k = 0.3$, and the friction coefficient of the right side is set to $\mu_k = 0$, the total mechanical energy will be maintained when the supporting-leg moves on the surface of $\mu_k = 0$ and decrease monotonously when it does on the surface of $\mu_k = 0.3$.

The configuration in **Fig. 2(a)** was detected at the time designated by Ⓐ in **Fig. 3**, and also **Figs. 2(b)** and **(c)** are the shapes at Ⓑ and Ⓒ. Since the equation of mo-

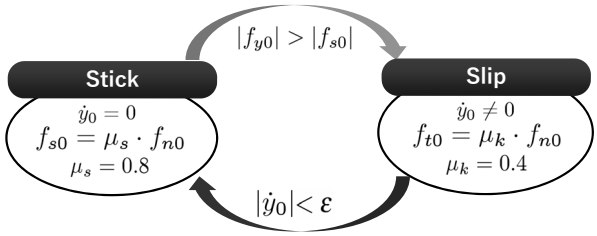

Fig. 4. Switch conditions of stick-slip motion.

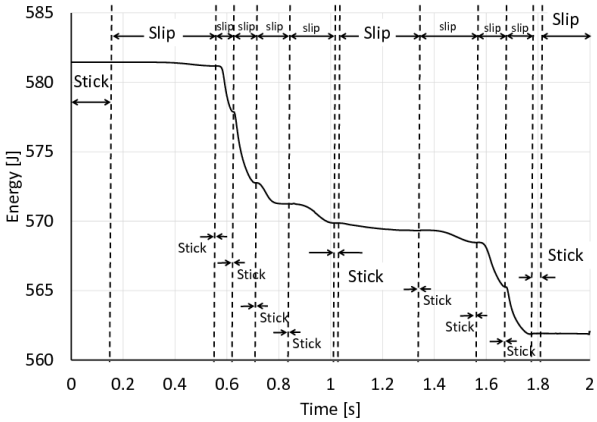

Fig. 5. Mechanical energy.

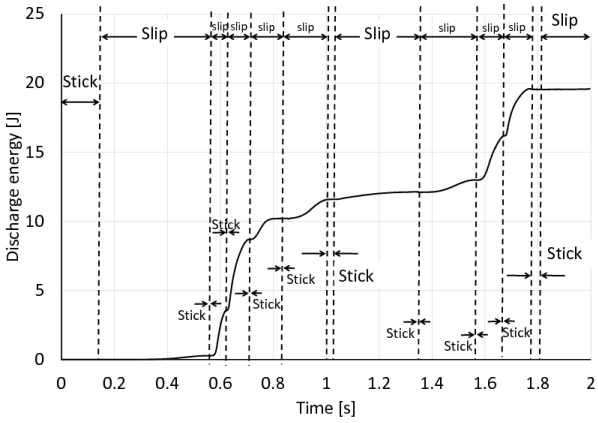

Fig. 6. Discharge of energy by friction.

tion used in this simulation represents the motion that the supporting-leg is kept to be contacting to the floor surface contact and the free-leg is not constraint, the free-leg can descend down below the ground surface as shown in **Figs. 2(b)** and **(c)**.

Figure 3 shows the result of the mechanical energy and the changes of the coefficient of friction when the supporting-leg is in a slip motion. From **Fig. 3**, when the supporting-leg is staying at the right part of ground ($\mu_k = 0$), the total of mechanical energy is saved. But when it is staying at the right part ($\mu_k = 0.3$), the mechanical energy is discharged by the effect of friction. So, it can be seen that supporting-leg slip model is feasible.

3.3.2. Simulation Including Stick-Slip

Another simulation with nonlinear friction between floor and foot has been prepared to examine a stick-slip motion that can verify the humanoid model further. The experiment conditions are shown as follows. The state (stick or slip) of supporting-leg that is dominated by the stick-slip conditions are shown in **Fig. 4**. When the driving force exerting to supporting-leg from dynamical coupling of humanoid nonlinear model f_{y0} is larger than the maximum static frictional force f_{s0}, the supporting-leg starts to slip. Here f_{n0} means the normal force exerting to the foot, and when the slip velocity of supporting-leg $|\dot{y}_0|$ is less than ε (a very small value $\varepsilon = 0.001$ m/s $= 1$ mm/s in this paper), the supporting-leg enters a stick state. During the supporting-leg in stick state, the coefficient of friction is set to $\mu_s = 0.8$, and when the supporting-leg is in slip state, the coefficient is set to $\mu_k = 0.4$. And the body of humanoid robot will fall freely without any viscous friction ($\boldsymbol{D} = \boldsymbol{0}$) and input torque ($\boldsymbol{\tau} = \boldsymbol{0}$).

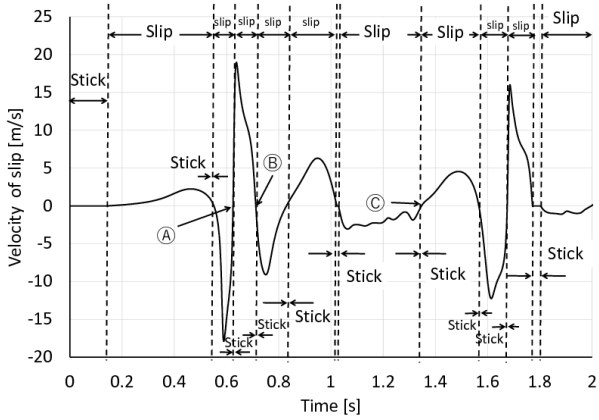

Fig. 7. Velocity of slip.

$$E_{discharge} = \int_0^t \mu_k \dot{y}_0^2 dt \quad \ldots\ldots\ldots \quad (30)$$

Figure 5 shows time profile of mechanical energy of humanoid's free-fall motion including the stick-slip motion, and **Fig. 6** shows the discharged energy caused by friction on floor, the calculation of discharged energy is shown in Eq. (30). Here, μ_k means the coefficient of friction when slipping, and when sticking the $E_{discharge}$ in Eq. (30) equal to zero since $\dot{y}_0$ is zero. In **Figs. 5** and **6**, when the supporting-leg is in the state of stick, the total of mechanical energy is remained unchanged. And the mechanical energy discharges while the the supporting-leg is slipping, and the value of discharged energy in **Fig. 6** is consistent with the result in **Fig. 5**.

Furthermore the velocity and the y-axis position of supporting-leg are shown in **Figs. 7** and **8**. **Fig. 7** shows that when the supporting-leg is in the state of stick, the velocity of slip equals to zero, and **Fig. 8** shows that the y-axis position is also not changed in time. And the discharge of energy depends on the velocity of slip. When the supporting-leg is slipping fast, the discharge of energy also gets a higher rate. Conversely, when supporting-leg is slipping very slow or stopping, the discharge of energy is also small or kept unchanged. So, from this simulation, it also can be seen that supporting-leg slip-stick model is feasible.

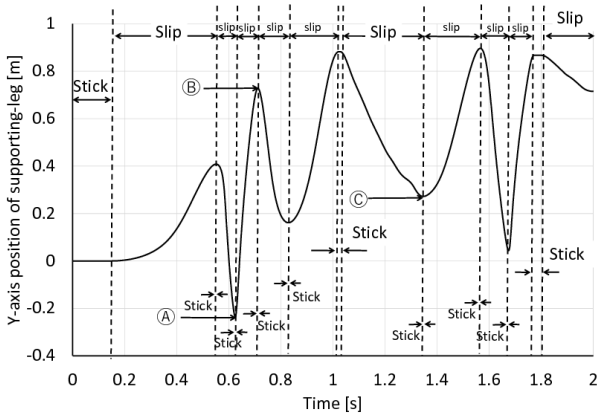

Fig. 8. y-position of supporting-leg.

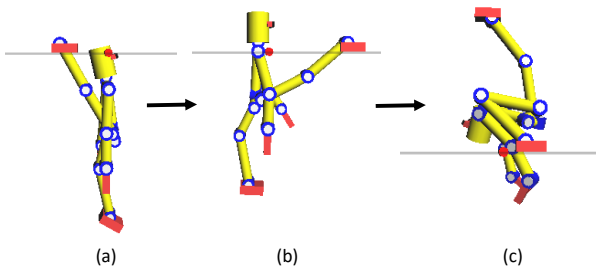

Fig. 9. Configurations during free-fall simulation shown in **Fig. 8**, (a) the configuration at time Ⓐ designated in **Fig. 8**, and (b) and (c) corresponds to time Ⓑ and Ⓒ.

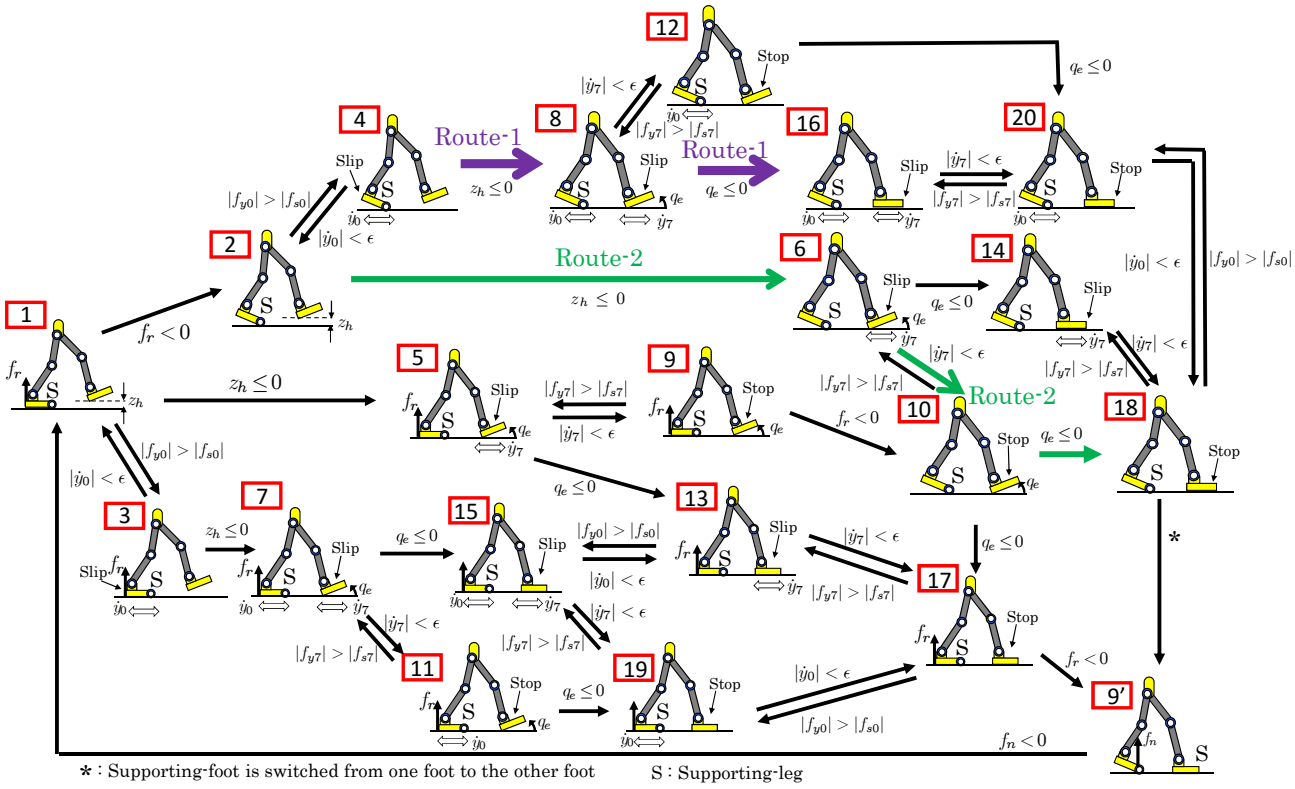

Fig. 10. States indicated by number enclosed by rectangular and gait transition including stick and slip motion.

Figure 9 shows their shapes of the humanoid while the simulated motion proceeds as shown in **Figs. 5–8**. The configuration in **Fig. 9(a)** was detected at the time designated by Ⓐ in **Figs. 7** and **8**, and also (b) and (c) are the shapes at Ⓑ and Ⓒ in the both figures.

4. Gait of Walking Model

4.1. Transition of Gait

In this research, humanoid walking with the transition of gaits state as shown in **Fig. 10**. And the route of state transition is determined by the walking motion of humanoid. In other words, it depends on the solution of the dynamics in Eq. (20). The dynamics and the state variable which depends on the gaits has been selected. And it will transit to the next state when the branching condition is satisfied. All of the walking dynamical models as in **Fig. 10** include the constrain conditions as shown in **Table 2**.

4.2. Switching Gaits

When the humanoid robot is walking, the gaits need to continue seamlessly by the conditions written at the upside position or downside of the arrows in **Fig. 10**. For example, in a simulation of common walking (route-2),

Table 2. Possible states for humanoid's walking, where the state number from (1) to (20) corresponds to the state number in rectangular in **Fig. 10**.

States in **Fig. 10**	State variables and constraining force and torque (Lagrange Multiplier)	Constraints (referrence)
(1)	$\boldsymbol{q} = [q_2, q_3, \cdots, q_{17}]^T$	
(2)	$\boldsymbol{q} = [q_1, q_2, \cdots, q_{17}]^T$	
(3)	$\boldsymbol{q} = [y_0, q_2, \cdots, q_{17}]^T$	
(4)	$\boldsymbol{q} = [y_0, q_1, \cdots, q_{17}]^T$	
(5)	$\boldsymbol{q} = [q_2, q_3, \cdots, q_{17}]^T, f_{nz}$	$C_{hz} = 0$
(6)	$\boldsymbol{q} = [q_1, q_2, \cdots, q_{17}]^T, f_{nz}$	$C_{hz} = 0$
(7)	$\boldsymbol{q} = [y_0, q_2, q_3, \cdots, q_{17}]^T, f_{nz}$	$C_{hz} = 0$
(8)	$\boldsymbol{q} = [y_0, q_1, q_2, q_3, \cdots, q_{17}]^T, f_{nz}$	$C_{hz} = 0$
(9)	$\boldsymbol{q} = [q_2, q_3, \cdots, q_{17}]^T, f_{nz}, f_{ny}$	$C_{hz}, C_{hy} = 0$
(10)	$\boldsymbol{q} = [q_1, q_2, \cdots, q_{17}]^T, f_{nz}, f_{ny}$	$C_{hz}, C_{hy} = 0$
(11)	$\boldsymbol{q} = [y_0, q_2, q_3, \cdots, q_{17}]^T, f_{nz}, f_{ny}$	$C_{hz}, C_{hy} = 0$
(12)	$\boldsymbol{q} = [y_0, q_1, q_2, q_3, \cdots, q_{17}]^T, f_{nz}, f_{ny}$	$C_{hz}, C_{hy} = 0$
(13)	$\boldsymbol{q} = [q_2, q_3, \cdots, q_{17}]^T, f_{nz}, \tau_n$	$C_{hz}, C_{fr} = 0$
(14)	$\boldsymbol{q} = [q_1, q_2, \cdots, q_{17}]^T, f_{nz}, \tau_n$	$C_{hz}, C_{fr} = 0$
(15)	$\boldsymbol{q} = [y_0, q_2, q_3, \cdots, q_{17}]^T, f_{nz}, \tau_n$	$C_{hz}, C_{fr} = 0$
(16)	$\boldsymbol{q} = [y_0, q_1, q_2, q_3, \cdots, q_{17}]^T, f_{nz}, \tau_n$	$C_{hz}, C_{fr} = 0$
(17)	$\boldsymbol{q} = [q_2, q_3, \cdots, q_{17}]^T, f_{ny}, f_{nz}, \tau_n$	$C_{hz}, C_{hy}, C_{fr} = 0$
(18)	$\boldsymbol{q} = [q_1, q_2, \cdots, q_{17}]^T, f_{ny}, f_{nz}, \tau_n$	$C_{hz}, C_{hy}, C_{fr} = 0$
(19)	$\boldsymbol{q} = [y_0, q_2, q_3, \cdots, q_{17}]^T, f_{ny}, f_{nz}, \tau_n$	$C_{hz}, C_{hy}, C_{fr} = 0$
(20)	$\boldsymbol{q} = [y_0, q_1, q_2, q_3, \cdots, q_{17}]^T, f_{nz}, f_{ny}, \tau_n$	$C_{hz}, C_{hy}, C_{fr} = 0$

the initial condition is set to state 2 shown in **Fig. 10**. When the free-leg touch the floor, meaning $z_h \leq 0$, the equation of motion is switched to state 6, and the free-leg start slipping. When the slipping stop, $|\dot{y}_7| < \varepsilon$, the state of motion is switched to state 10. Then the gait state will be switched continually to state 18, 9', 1 and goes back to state 2 by their switching conditions. The state number in rectangular box in **Fig. 10** corresponds to the number of states in **Table 2**.

In this paper, gaits in **Fig. 11** are verified by using the mechanical energy conservation law as the same in Section 3. Two verification experiments about the gaits switching have been prepared. The switching route-1,2 in **Fig. 10** is used. The route-1 actually shows a common pattern to fall to the ground. And the route-2 shows the common bipedal walking. In the route-1 and 2, the viscous friction coefficient of each joints and the friction coefficient the foot and the ground are set to zero. So the transition of state in route-1 and 2 are transferred as shown in **Fig. 11**. Because the gait number (6) in the route-2 occur in a very short moment after the foot contact to the ground, and it switch to the gait (10) immediately. So, in the route-2, the gait (6) not discussed in this experiment.

Figure 12 shows the shapes of humanoid during the switching simulation of route-1. From **Fig. 12**, the initial state of gaits is (4). When the heel and toe of free-leg bumping with the floor, the state is switched to number (8) and (16) continually.

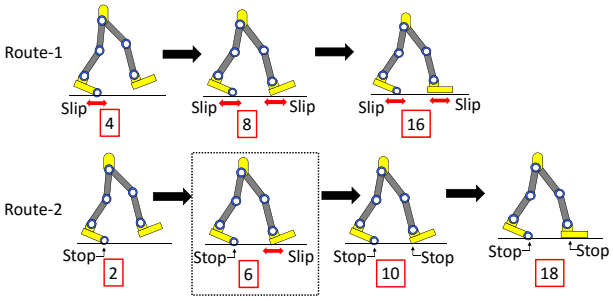

Fig. 11. Experimental of switching of gait.

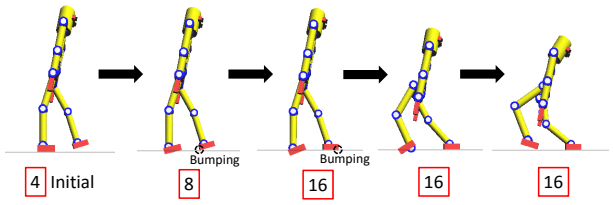

Fig. 12. Experimental simulation of switching route-1.

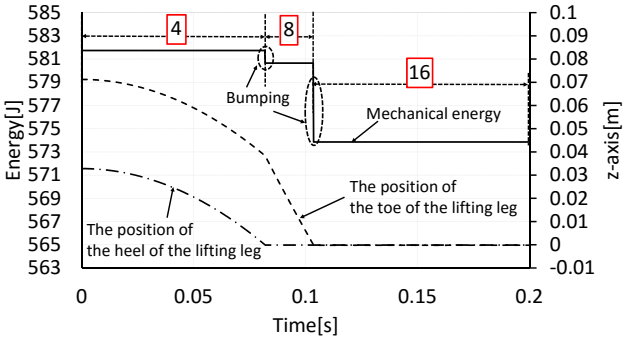

Fig. 13. The result of route-1.

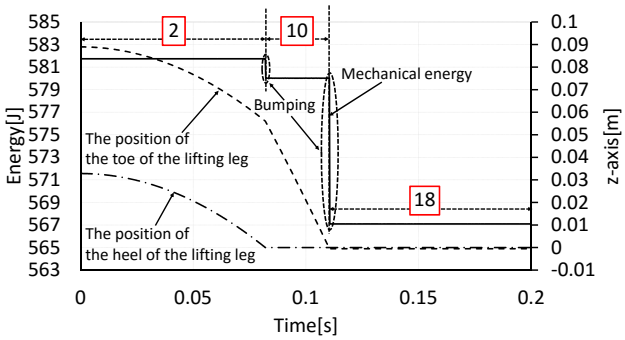

Fig. 14. The result of route-2.

The result about the mechanical energy conservation law of the route-1 and 2 are shown in **Figs. 13** and **14**. From these two figures, when the foot is contact with the ground, the mechanical energy has been dissipated by bumping, but in each gait, the mechanical energy has been kept. So, considering that the mechanical energy conservation law has been satisfied in each gaits, the gaits switching models are verified to be noncontradiction.

5. Conclusion

In this paper, we have proposed a walking model of humanoid including slipping, bumping, surface-contacting and point-contacting of foot, whose dynamical equation is derived by Newton-Euler method with constraint condition.

References:

[1] S. Kajita, M. Morisawa, K, Miura, S. Nakaoka, K. Harada, K. Kaneko, F. Kanehiro, and K. Yokoi, "Biped Walking Stabilization Based on Linear Inverted Pendulum Tracking," Proc. of IEEE/RSJ Int. Conf. on Intelligent Robots and Systems, pp. 4489-4496, 2010.

[2] H. Dau, C. Chew, and A. Poo, "Proposal of Augmented Linear Inverted Pendulum Model for Bipedal Gait Planning," Proc. of IEEE/RSJ Int. Conf. on Intelligent Robots and Systems, pp. 172-177, 2010.

[3] J. H. Park and K. D. Kim, "Biped walking robot using gravity-compensated inverted pendulum mode and computed torque control," Proc. of IEEE Int. Conf. on Robotics and Automation, Vol.4, pp. 3528-3593, 1998.

[4] P. B. Wieber, "Trajectory free linear model predictive control for stable walking in the presence of strong perturbations," Proc. of Int. Conf. on Humanoid Robotics, 2006.

[5] P. B. Wieber, "Viability and predictive control for safe locomotion," Proc. of IEEE/RSJ Int. Conf. on Intelligent Robots and Systems, 2008.

[6] A. Herdt, N. Perrin, and P. B. Wieber, "Walking without thinking about it," Proc. of IEEE/RSJ Int. Conf. on Intelligent Robots and Systems, pp. 190-195, 2010.

[7] Y. Huang, B. Chen, Q. Wang, K. Wei, and L. Wang, "Energetic efficiency and stability of dynamic bipedal walking gaits with different step lengths," Proc. of IEEE/RSJ Int. Conf. on Intelligent Robots and Systems, pp. 4077-4082, 2010.

[8] M. Sobotka and M. Buss, "A Hybrid Mechatronic Tiliting Robot: Modeling, Trajectories, and Control," Proc. of the 16th IFAC World Congress, 2005.

[9] T. Wu, T. Yeh, and B. Hsu, "Trajectory Planning of a One-Legged Robot Performing Stable Hop," Proc. of IEEE/RSJ Int. Conf. on Intelligent Robots and Systems, pp. 4922-4927, 2010.

[10] Y. Nakamura and K. Yamane, "Dynamics of Kinematic Chains with Discontinuous Changes of Constraints—Application to Human Figures that Move in Contact with the Environments—," J. of RSJ, Vol.18, No.3, pp. 435-443, 2000 (in Japanese).

[11] J. Nishiguchi, M. Minami, and A. Yanou, "Iterative calculation method for constraint motion by extended Newton-Euler method and application for forward dynamics," Trans. of the JSME, Vol.80, No.815, 2014.

[12] R. Featherstone and D. Orin, "Robot Dynamics: Equations and Algorithms," IEEE Int. Conf. on Robotics and Automation, pp. 826-834, 2000.

[13] H. Hemami and B. F. Wyman, "Modeling and Control of Constrained Dynamic Systems with Application to Biped Locomotion in the Frontal Plane," IEEE Trans. on Automatic Control, AC-24-4, pp. 526-535, 1979.

[14] T. Feng, J. Nishiguchi, X. Li, M. Minami, A. Yanou, and T. Matsuno, "Dynamical Analyses of Humanoid's Walking by using Extended Newton-Euler Method," 20st Int. Symp. on Artificial Life and Robotics (AROB 20st), 2015.

[15] Y. Kobayashi, M. Minami, A. Yanou, and T. Maeba, "Dynamic Reconfiguration Manipulability Analyses of Humanoid Bipedal Walking," IEEE Int. Conf. on Robotics and Automation (ICRA), pp. 4764-4769, 2013.

[16] T. Aoyama, Y. Hasegawa, K. Sekiyama and T. Fukuda, "Stabilizing and Direction Control of Efficient 3-D Biped Walking Based on PDAC," 2009 IEEE/ASME Trans. on Mechatronics, pp. 712-718, 2009.

[17] T. Sugihara and Y. Nakamura, "Whole-body Cooperative COG Control through ZMP Manipulation for Humanoid Robots," Proc. of the 2nd Int. Symp. on Adaptive Motion of Animals and Machines, SaP-III-4, 2003.

[18] C. Chevallereau, J. W. Grizzle, and C.-L. Shih, "Asymptotically Stable Walking of a Five-Link Underactuated 3-D Bipedal Robot," IEEE Trans. on Robotics, Vol.25, No.1, February 2009.

[19] Y. Ueda and M. Henmi, "An experimental and analytical study on Stick-Slip motions," Technical Report of lEICE, CAS Vol.96, pp. 41-48, 1996.

[20] L. R. Tokashiki, T. Fujita, and T. Kagawa, "Stick-Slip Motion in Pneumatic Cylinders Driven by Meter-out Circuit 1st Report, Friction Characteristics and Stick-Slip Motion ," Trans. of The Japan Hydraulics & Pneumatics Society, Vol.30, No.4, pp. 110-117, 1999.

[21] K. Nakano, "A Guideline of Machinary Design for Preventing Stick-Slip," Nippon Gomu Kyokaishi, Vol.80, No.4, pp. 134-139, 2007.

[22] M. Kouchi, M. Mochimaru, H. Iwasawa, and S. Mitani, "Anthropometric database for Japanese Population 1997–98," Japanese Industrial Standards Center (AIST, MITI), 2000.

[23] T. Maeba, M. Minami, A. Yanou, and J. Nishiguchi, "Dynamical Analyses of Humanoid's Walking by Visual Lifting Stabilization Based on Event-driven State Transition," 2012 IEEE/ASME Int. Conf. on Advanced Intelligent Mechatronics Proc., pp. 7-14, 2012.

Name:
Xiang Li

Affiliation:
Ph.D. Student, Graduate School of Natural Science and Technology, Okayama University

Address:
3-1-1 Tsushimanaka, Okayama 700-8530, Japan

Brief Biographical History:
2014- Master Course Student, Graduate School of Natural Science and Technology, Okayama University
2016- Ph.D. Student, Graduate School of Natural Science and Technology, Okayama University

Main Works:
• "Dynamical Modeling of Humanoid with Nonlinear Floor Friction," 21st Int. Symp. on Artificial Life and Robotics, B-Con Plaza Beppu, January 20-22, 2016.
• "Iterative Calculation Method for Constraint Motion by Extended Newton-Euler Method and Application for Forward Dynamics," IEEE/SICE Int. Symp. on System Intergaration, SuE5.4, Meijo University, Nagoya, December 11-13, 2015.

Membership in Academic Societies:
• The Society of Instrument and Control Engineers (SICE)
• The Robotics Society of Japan (RSJ)

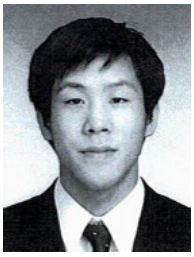

Name:
Hiroki Imanishi

Affiliation:
Master Course Student, Graduate School of Natural Science and Technology, Okayama University

Address:
3-1-1 Tsushimanaka, Okayama 700-8530, Japan

Brief Biographical History:
2014- Master Course Student in Graduate School of Natural Science and Technology, Okayama University

Main Works:
• "Knee Constraint Effects of Bipedal Walking by Visual-lifting Approach," The Society of Instrument and Control Engineers, pp. 756-761, September 9–12, 2014.

Name:
Mamoru Minami

Affiliation:
Professor, Graduate School of Natural Science and Technology, Okayama University

Address:
3-1-1 Tsushimanaka, Okayama 700-8530, Japan

Brief Biographical History:
1990- Doctoral Course Student in the Graduate School of Natural Science and Technology, Kanazawa University
1994- Associate Professor, Department of Mechanical Engineering, University of Fukui
2002- Professor, Department of Human and Artificial Intelligence Systems, University of Fukui
2010- Professor, Graduate School of Natural Science and Technology, Okayama University

Main Works:
• "Reconfiguration Manipulability Analyses for Redundant Robots," Trans. of the ASME, J. of Mechanisms and Robotics, Vol.5, No.4, pp. 1-16, 2013.
• "Visual Servoing to catch fish Using Global/local GA Search," IEEE/ASME Trans. on Mechatronics, Vol.10, No.3, pp. 352-357, 2005.

Membership in Academic Societies:
• The Institute of Electrical and Electronics Engineers (IEEE)
• The Japanese Society of Mechanical Engineers (JSME)
• The Society of Instrument and Control Engineers (SICE)
• The Robotics Society of Japan (RSJ)

Name:
Takayuki Matsuno

Affiliation:
Lecturer of The Graduate School of Natural Science and Technology, Okayama University

Address:
3-1-1 Tsushimanaka, Okayama 700-8530, Japan

Brief Biographical History:
2000- Received the M.E. degree from Nagoya University
2005- Received Dr.Eng. from Nagoya University
2004- Joined the Nagoya University
2006- Joined the Toyama Prefectural University

Main Works:
• "Manipulation of Deformable Linear Objects using Knot Invariants to Classify the Object Condition Based on Image Sensor Information," IEEE/ASME Trans. on Mechatronics, Vol.11, Issue 4, pp. 401-408, 2006.
"Development of Production Robot System that can Assemble Products with Cable and Connector," J. of Robotics and Mechatronics, Vol.23, No.6, pp. 939-950, 2011.

Membership in Academic Societies:
• The Institute of Electrical and Electronics Engineers (IEEE) Robotics and Automation Society (RAS)
• The Japan Society of Mechanical Engineers (JSME)
• The Robotics Society of Japan (RSJ)
• The Society of Instrument and Control Engineers (SICE)

Name:
Akira Yanou

Affiliation:
Associate Professor, Department of Radiological Technology, Kawasaki College of Allied Health Professions

Address:
316 Matsushima, Kurashiki, Okayama 701-0194, Japan

Brief Biographical History:
2001- Ph.D. in Engineering, Okayama University
2002- Assistant Professor, Faculty of Engineering, Kinki University
2004- Lecturer, Faculty of Engineering, Kinki University
2009- Assistant Professor, Graduate School of Natural Science and Technology, Okayama University
2016- Associate Professor, Department of Radiological Technology, Kawasaki College of Allied Health Professions

Main Works:
• "Autonomous docking control of visual-servo type underwater vehicle system aiming at underwater automatic charging," Trans. of the JSME (in Japanese), Vol.81, No.832, 15-00391, Dec. 2015.

Membership in Academic Societies:
• The Institute of Electrical and Electronics Engineers (IEEE)
• The Japan Society of Mechanical Engineers (JSME)
• THe Society of Instrument and Control Engineers (SICE)
• The Institute of Systems, Control and Information Engineers (ISCIE)
• Japanese Society of Radiological Technology